



Article

Reactive Polymer Composite Microparticles Based on Glycidyl Methacrylate and Magnetite Nanoparticles

Agnieszka Bukowska , Karol Bester , Sylwia Flaga and Wiktor Bukowski *

Faculty of Chemistry, Rzeszów University of Technology, al. Powstańców W-wy 6, 35-959 Rzeszów, Poland
* Correspondence: wbuk@prz.edu.pl

Abstract: The modified suspension polymerization technique has been used for the preparation of composite microparticles from the mixture of glycidyl methacrylate (GMA), styrene (S), and divinylbenzene (DVB) in the presence of hydrophobized Fe_3O_4 nanoparticles. The obtained polymer microspheres were characterized using different instrumental and physicochemical techniques, modified with a zero-order PAMAM dendrimer, and impregnated with palladium(II) acetate solutions to immobilize palladium(II) ions. The resulting materials were preliminarily examined as catalysts in the Suzuki reaction between 4-bromotoluene and phenylboronic acid. It was found that the addition of magnetite particles to the composition of monomers provided polymer microparticles with embedded magnetic nanoparticles. The composite microparticles obtained showed a complex, multi-hollow, or raspberry-like morphology. After their modification, they could serve as recyclable catalysts for reactions that include both 4-bromotoluene and several other aryl bromides.

Keywords: polymer composite microparticles; magnetic nanoparticles; multi-hollow morphology; Suzuki cross coupling reaction

1. Introduction



Citation: Bukowska, A.; Bester, K.; Flaga, S.; Bukowski, W. Reactive Polymer Composite Microparticles Based on Glycidyl Methacrylate and Magnetite Nanoparticles. *Solids* **2024**, *5*, 151–171. <https://doi.org/10.3390/solids5010011>

Academic Editor: Chee Yoon Yue

Received: 22 December 2023

Revised: 11 February 2024

Accepted: 13 March 2024

Published: 18 March 2024



Copyright: © 2024 by the authors. Licensee MDPI, Basel, Switzerland. This article is an open access article distributed under the terms and conditions of the Creative Commons Attribution (CC BY) license (<https://creativecommons.org/licenses/by/4.0/>).

It is well known that epoxides that have the three-membered ring in their structure can interact with a wide range of reagents to form new valuable products [1]. When epoxy groups are part of insoluble materials (organic, inorganic, hybrid, or composite), their presence allows the materials to be easily modified to obtain new materials with properties tuned to specific applications. For example, glycidyl methacrylate polymers were applied for the immobilization of enzymes [2,3], as drug transport systems [4,5], as sorbents in some types of chromatography, for the recovery of metals from aqueous solutions [6,7], and as catalyst supports [8,9].

Magnetite (Fe_3O_4) nanoparticles also have great research interest due to their potential applications in numerous areas, such as, for example, mineral separation [10], heat transfer [11], electrophotography [12], and different biomedical applications (magnetic resonance imaging (MRI), gene therapy, hyperthermia, chemotherapy, and controlled drug transport) [13–19].

There are different methods for producing magnetite nanoparticles (MNPs), including co-precipitation, sol-gel, microemulsion, and different thermal and hydrothermal methods [20–22]. One of the most widely used Fe_3O_4 synthesis methods, due to its simplicity, is the co-precipitation of Fe(II) and Fe(III) ions from water solutions with a base performed in an inert gas atmosphere [19]. Aqueous solutions of ammonia or sodium hydroxide are most often used for this purpose. Using co-precipitation methods, particles of a wide range of diameters and shapes can be produced depending on the salts used, the ratio of Fe(II) and Fe(III) ions, the ionic strength, temperature, pH reaction mixture, and the stirring speed [20–23]. To minimize particle sizes and prevent excessive particle agglomeration, chelating compounds are used, such as citric, gluconic, or oleic acids [21].

Unmodified iron oxide MNPs, due to their anisotropic and dipolar properties and their ability to become magnetized, easily aggregate to form large clusters. Therefore, before further use, the surfaces of MNPs are often modified in addition to the use of different chelates [20,24].

Polymers are characterized by good coating properties, and therefore, they are willingly used in the preparation of magnetic composite materials. Polymer coatings can be used to prevent MNPs from aggregation and agglomeration, increase compatibility between MNPs and the aqueous environment, prevent their surface from oxidizing, reduce toxicity, prevent direct contact of the magnetic substance with the environment, increase colloidal and chemical stability, and facilitate storage or transportation. At the same time, the modification of the iron oxide surface with polymers can expand the scope of the use of materials that have embedded magnetic nanoparticles with completely new applications, such as water purification [25–27], cell separation and detection [28,29], proteins, nucleic acids, enzymes [30–32], and catalyst immobilization [33–35], as well as in various fields of biotechnology and biomedicine, for example, as systems for targeted drug delivery, DNA isolation, and magnetic hyperthermia targeted drug delivery, and magnetic resonance imaging (MRI) [18,35–38].

Polymer magnetic microspheres are macromolecular systems that exhibit the properties of both types of materials. For example, such materials can be isolated easily and quickly using an external magnetic field without the need to use demanding processes such as filtration and centrifugation. The presence of polymers in the composites, in addition to stabilizing MNPs, provides unique physical and chemical properties such as, for example, biocompatibility and reactive functional groups, allowing the composite to undergo further chemical modification to tune the properties of magnetic composites for specific applications.

Several methods are used to obtain polymers in the form of particles. Precipitation, emulsion, and suspension polymerization methods are the most explored [39]. One of the main criteria for selecting the proper method is the size of the particles provided. Depending on the method used, the diameters of the polymer particles provided range from ~50 nm to 2 mm.

To encapsulate magnetic particles within polymeric materials, emulsion [40,41], mini-emulsion [42–44], dispersion [45,46], suspension [47–49], micro-suspension [50], precipitation [51], and in situ polymerization [52] and in situ coprecipitation [53] were previously used. Suspension polymerization and its modifications are among the most frequently used methods in the preparation of polymer magnetic microspheres. For example, Wang et al. [48] used modified suspension polymerization to obtain porous magnetic microspheres from methyl methacrylate (MMA), divinylbenzene (DVB), and iron oxide coated with oleic acid (OA). Based on TEM and SEM analyses, most of the Fe₃O₄-OA particles were found to be within the copolymer network, and the composite particles obtained had a spherical shape and porous structure. Liu et al. also used the modified suspension copolymerization method to produce magnetic polymer microspheres [54]. Styrene, divinylbenzene, and glycidyl methacrylate (GMA) were used in this case as comonomers with the magnetic fluid prepared by the precipitation method. The composite microspheres provided in this case showed a much smaller size (4–7 μm) compared to traditional suspension polymerization methods and a narrower size distribution. The glycidyl groups introduced into the composite materials with GMA molecules allowed them to be used to bind proteins or enzymes.

Since suspension polymerization, as a method of preparing epoxy functionalized terpolymers from mixtures of styrene, divinylbenzene, and glycidyl methacrylate, was also previously used in our laboratory to develop easily modifiable gel-type polymer microparticles [55–57], an idea to use magnetite nanoparticles to modify the morphology of the gel-type polymer beads was presented. It was expected that the addition of magnetite nanoparticles in the form of dispersion in toluene to the monomer composition diluted with an organic solvent will make it possible to obtain new modifiable composite materials

for catalytic or sorption purposes. Unexpectedly, microparticles with unique multi-hollow or raspberry-like morphologies, characterized by very slight magnetic properties, were obtained when the polymerization conditions were optimized.

2. Experimental Part

2.1. Materials

The chemicals used in this work were commercially available from Sigma-Aldrich (Sigma Aldrich Chemie GmbH, München, Germany), Merck (Darmstadt, Germany), Fluka (Buchs, Switzerland), or POCH (Gliwice, Poland), and were used as received unless otherwise stated. Monomers, styrene (S, >99%), divinylbenzene (DVB, 80%), and glycidyl methacrylate (GMA, 97%) were purified from inhibitors by extraction with aqueous solution of 5% NaOH and 20% NaCl, washed 3–4 times with deionized water, and dried under anhydrous magnesium sulfate prior to use.

2.2. Characterization

The resin morphology was estimated using stereomicroscopes (Leica M205A, Leica Microsystems, GmbH, Wetzlar, Germany, equipped with a digital camera and focus stacking software and Motic SMZ-143, Motic, Germany, equipped with a digital camera) and a VEGA3 TESCAN scanning electron microscope (TESCAN Brno, Brno, Czech Republic) equipped with an X-ray energy dispersive (EDS) system. FTIR spectra were recorded using a Thermo Scientific Nicolet 8700 spectrometer (as KBr pallets) or a FTIR Nicolet iN10MX microscope equipped with a micro compression diamond cell (Thermo Scientific, Waltham, MA, USA). Samples for the FTIR microscopy analyses were prepared by flattening polymer beads between a pair of diamond windows of the micro compression cell.

The particle size distribution and average particle diameters were analyzed using dynamic light scattering (DLS) techniques. Zetasizer Nano ZS and Mastersizer 2000E instruments from Malvern Instruments Ltd. (Malvern, UK) were applied. The microparticle analyzer was equipped with a Hydro MU wet sample dispersion unit. The DLS measurements of particles were performed using isopropyl alcohol as a dispersive medium. The samples of the examined particles were sonicated for 15 min before each measurement.

TGA analysis was performed using a METTLER TOLEDO TGA/DSC 1 analyzer (METTLER TOLEDO AG, Analytical, Schwerzenbach, Switzerland). Samples were heated from 25 to 600 °C (10 °C/min) in a nitrogen atmosphere (50 mL N₂/min). The epoxy group content in the beads was determined using the modified Jay method [55]. The nitrogen content in the products was determined using the Kjeldahl method.

To determine the swelling capacity of the obtained composite particles, approximately 0.2 g of samples of synthesized microparticles was placed in 2 mL syringes and swelled in a series of solvents or solvent mixed systems. Samples were washed with methanol between subsequent measurements. After complete swelling of the particles, excess solvent was removed using the syringe plunger, and then the mass occupied by the swollen polymers was read, and the weight gain per 1 g of dry polymers was calculated using the following formula:

$$S = \frac{m_k - m_p}{\rho \cdot m_p}$$

where

m_p —mass of dry polymer [g];

m_k —mass of swollen polymer [g];

ρ —solvent density [g/mL].

The palladium content in the obtained composite microparticles was determined using an ICP-OES spectrometer. ICP OES analyses were performed at $\lambda = 217.809$ and 240.488 nm (Fe) and at 248.892 and 340.458 nm (Pd) using a Horiba Jobin Yvon Optima 2 ICP-OES spectrometer (Horiba, Jobin Yvon, France). Particle samples (~5–10 mg) were mineralized in nitric acid (69 wt.%, 5.0 mL) using a Plazmatronika Uni Claver II microwave mineralizer (Wrocław, Poland).

GC analyzes were performed using an Agilent 7890 GC chromatograph (Agilent, Palo Alto, CA, USA) with a split-splitless injector, a flame ionization detector, an auto-sampler, and a HP-5 capillary column. Analytical solutions were prepared by dissolving 20 mg samples taken from the reaction mixtures in 0.5 mL of tetrahydrofuran (THF). Nonane was used as a standard.

2.3. General Procedure of Preparation of Glycidyl-Functionalized Polymer Composite Microparticles

A three-neck flask with a capacity of 250 mL equipped with a mechanical stirrer, a thermometer, dropping funnel, an argon supply system (an argon balloon), and a heating mantle were used to react 2.35 g (0.008 mol) $\text{FeSO}_4 \cdot 7\text{H}_2\text{O}$ and 2.45 g (0.015 mol) FeCl_3 dissolved in 100 mL of deionized water with 25 mL of 28 wt.% ammonia solution. The ammonia solution was added dropwise under an argon atmosphere at room temperature. The reaction mixture was stirred intensively during this operation. Then, the mixture was heated to 80 °C, and 1 mL of oleic acid was added very slowly dropwise. The mixing was continued at 80 °C for 1 h upon allowing the reaction mixture to cool to ambient temperature. Then, black precipitate was extracted twice with toluene (2×50 mL) to transfer the hydrophobic Fe_3O_4 particles provided from water to toluene. The resulting toluene dispersion was dried by azeotropic distillation using a Dean–Stark apparatus and then diluted with dry toluene to obtain the final concentration of 10 mg of Fe_3O_4 in 1 mL of toluene. The final black dispersion was applied for the synthesis of polymer particles. To perform the polymerization, a cylindrical-shaped 100 mL reactor equipped with a heating coat, a reflux condenser, and a mechanical stirrer was used. Monomers (20 mol% GMA, 77 mol% S and 3 mol% DVB), an initiator (benzoyl peroxide), and the dispersion of $\text{Fe}_3\text{O}_4@\text{OA}$ in toluene were mixed, diluted with toluene, and then sonicated using an ultrasonic bath for 15 min. The organic phase prepared in this manner was then dispersed slowly in a poly(vinyl alcohol) water solution (1% PVA, 18–88, Fluka). A 100 mL cylindrical glass reactor equipped with a heating coat, a mechanical stirrer, and a reflux condenser was used to perform the polymerization. The stirring rate was adjusted to 350 rpm. The mixture reacted under an argon atmosphere at 70 °C for 2 h and at 80 °C for 6 h. After the reaction, the mixture was cooled to ambient temperature, and it was poured into a glass beaker with water. The polymer particles were then washed several times with water until a clear filtrate was obtained, and then filtered on a Büchner funnel. The particles were then transferred to a Soxhlet apparatus, where extraction with acetone was carried out for 6 h. Subsequently, the microbeads were resuspended in methanol, filtered, and dried at 40 °C under reduced pressure.

Detailed synthesis conditions and characteristics of polymer products are presented in Table 1.

Table 1. Polymerization conditions and polymer particle characteristics.

Entry	Abbr.	Fe_3O_4 , wt. %	Average Size, μm	Diameter Range, μm	Fraction, %	Fe Content		
						Calculated, wt. %	Determined, wt. %	Modification Degree, %
1	1a	-	211	100–448	100	-	-	-
2	1b	0.05	272	142–632	100	0.036	0.013	36.0
3	1c	0.10	328	159–710	100	-	-	-
4	1d	0.25	386	159–1002	95.1	0.181	0.048	26.5
5	1e	0.50	256	112–633	95.7	0.361	0.068	18.8
6	1f	0.75	298	142–633	100	0.542	0.095	17.5
7 *	1g	0.50	247	100–564	100	-	-	-
8 **	1h	0.50	173	50–448	88.8	-	-	-

Other parameters: GMA (20 mol%); DVB (3 mol%); S (77 mol%); an initiator (BPO) (1 wt.%); water phase (1 wt.% PVA solution); monomers/toluene ratio (1:1) (v:v); stirring rate (350 rpm); * 500 rpm; ** 600 rpm.

2.4. Post-Modification of Composite Microparticles with PAMAM Type of Polyamidoamine

Composite microparticles (**1d** or **1e**, 0.5 g) were placed in a 50 mL glass reactor equipped with a heating coat and swollen in 10 mL of the mixed solvent of DMF:MeOH (3:1; *v:v*). Polyamidoamine (PAMAM) (3 eq) dissolved in 5 mL of the same mixed solvent was added to the swelled microparticles. The reactor was blown with argon, sealed, and placed on a rotary shaker and heated to 70 °C. The reaction mixture was shaken at this temperature for 48 h. After the post-reaction mixture was cooled, the modified particles were filtered and washed first with the mixture of DMF:MeOH, and then washed several times with a mixture of CH₂Cl₂:MeOH to remove excessive polyamidoamine. The final products were dried to constant weight in a vacuum dryer.

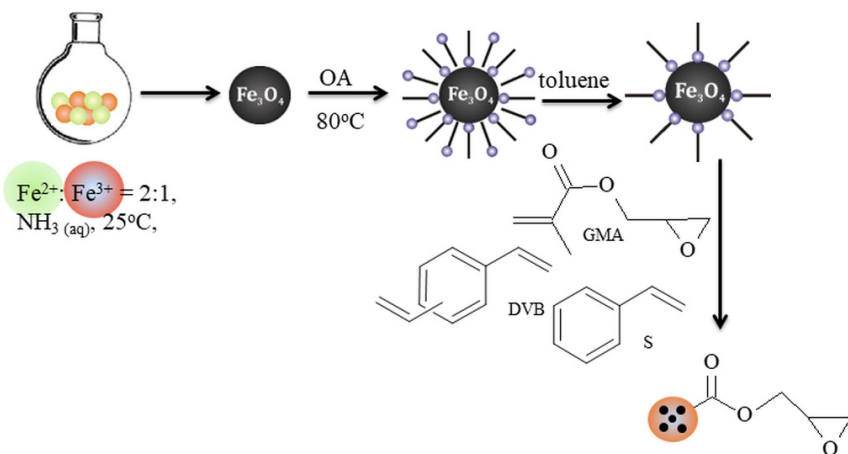
2.5. Palladium(II) Acetate Immobilization

Samples of polyamine-modified microparticles (0.180 g of **2d** and 0.186 g of **2e**) were placed in 10 mL screw cap glass vials and pre-swollen in 0.5 mL of THF. Separately, solutions of palladium(II) acetate were prepared in 1.5 mL of THF (44.7 mg for **2d** and 54.32 mg for **2e**), which were then added to the swollen resins. The vials with the reaction mixtures were sealed, placed on a vibratory rotating shaker, and shaken for 24 h at room temperature. After this time, the modified microparticles were transferred to PP syringes equipped with Luer valves and cotton wool filters and washed with water and THF. The products (**3**) were dried in a vacuum oven at 40 °C for at least 48 h.

3. Results and Discussion

3.1. Preparation of Epoxy Functionalized Composite Microparticles

Suspension polymerization of the monomer composition containing 20 mol% glycidyl methacrylate (GMA), 77 mol% styrene (S), 3 mol% divinylbenzene (DVB), and benzoyl peroxide (BPO, as a polymerization initiator) diluted with a proper organic solvent provided strongly swellable and easily modifiable gel-type polymer microparticles [55]. In this work, magnetite nanoparticles were applied to modify the previously developed procedure and obtain epoxy-functionalized swellable polymer–inorganic composite microparticles (Scheme 1).



Scheme 1. Synthesis of GMA-S-DVB terpolymers with embedded Fe_3O_4 nanoparticles.

Hydrophobized magnetite particles were prepared by precipitating Fe_3O_4 from the water solution of $\text{FeSO}_4 \cdot 7\text{H}_2\text{O}$ (1 eq.) and FeCl_3 (2 eq.) with ammonia and modifying the surfaces of the initially precipitated particles with oleic acid (OA). Hydrophobic molecules of OA cover the surface of the formed nanoparticles, limit their agglomeration, and allow $\text{Fe}_3\text{O}_4@\text{OA}$ particles to be transferred to organic solvents. In this work, toluene was used to obtain $\text{Fe}_3\text{O}_4@\text{OA}$ particle fluid. The provided particles were quantitatively transferred to toluene, and the resulting black fluid contained nanosized magnetic particles. Figure 1

presents the size distribution of the nanoparticles in a fluid sample dispersed in isopropyl alcohol determined using a dynamic light scattering (DLS) technique.

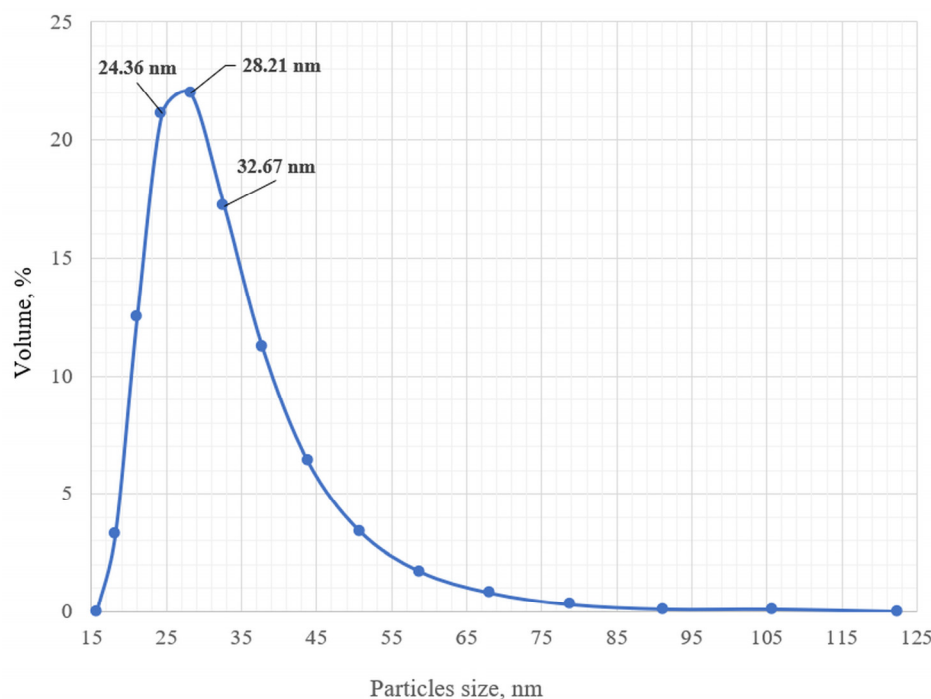


Figure 1. Size distribution of $\text{Fe}_3\text{O}_4@\text{OA}$ particles in toluene magnetic fluid.

The obtained toluene magnetite dispersion was used in an amount of 0.05–0.75 wt.% $\text{Fe}_3\text{O}_4@\text{OA}$ by weight with respect to the monomers. To achieve a good swelling capacity of the final composite microparticles and to provide compatibility with $\text{Fe}_3\text{O}_4@\text{OA}$ particles, toluene was applied as a diluent for the monomer composition instead of the previously used cyclohexanol/octanol mixture [55,58].

Initially, polyvinylpyrrolidone K-90 solutions (PVP, 1–3 wt.%) were used as a dispersive medium; however, they did not provide the appropriate conditions to stabilize the suspension of monomer compositions with toluene and $\text{Fe}_3\text{O}_4@\text{OA}$ nanoparticles. As a result, it was rather impossible to separate polymer particles from irregularly shaped impurities that also formed abundantly during polymerization. A clear improvement in the form of the polymer particles was observed when the PVP solutions were replaced by poly(vinyl alcohol) (PVA, 1 wt.%) solution.

The polymerization conditions were then optimized by changing the ratios of water to organic phases and toluene to monomers. The best results were obtained for the ratios of 8:1 and 2:1, respectively. For these conditions, a series of polymerization experiments were performed in which the concentration of $\text{Fe}_3\text{O}_4@\text{OA}$ and the stirring rate were changed. The brownish particles provided as a result were characterized by the broad size dispersity compared to products of classical suspension polymerization (Table 1). Furthermore, the average diameter of the particles increased by approximately 60 μm when only 0.05 wt.% $\text{Fe}_3\text{O}_4@\text{OA}$ was added to the monomer composition (Figure 2, Table 1, entry 2). An increase in the amount of $\text{Fe}_3\text{O}_4@\text{OA}$ to 0.25 wt.% entailed a further increase in the average diameter of the polymer particles (Table 1, entry 4). It also resulted in an increase in the dispersity of the particle size. Further doubling the concentration of $\text{Fe}_3\text{O}_4@\text{OA}$ (Table 1, entry 5) caused a decrease in the average diameter of the final polymer particles. However, this factor did not have a substantial influence on the particle size distribution. A slight increase in the particle diameter and a decrease in dispersity was observed when 0.75 wt.% $\text{Fe}_3\text{O}_4@\text{OA}$ was used (Table 1, entry 6). A similar effect was obtained by increasing the stirring rate from 350 to 500 rpm (Figure 3, Table 1, entry 7). However, a further increase in the stirring rate to 600 rpm caused an increase in the dispersity of particle size (Table 1, Entry 8).

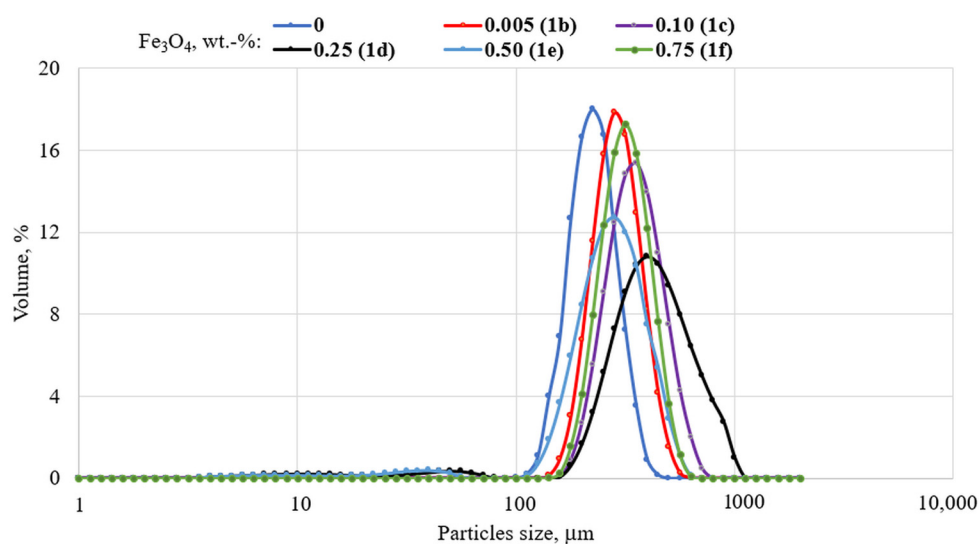


Figure 2. Size distributions of polymer particles prepared using 20 mol% GMA, 77 mol% S, and 3 mol% DVB and $\text{Fe}_3\text{O}_4@\text{OA}$ particles as an additive.

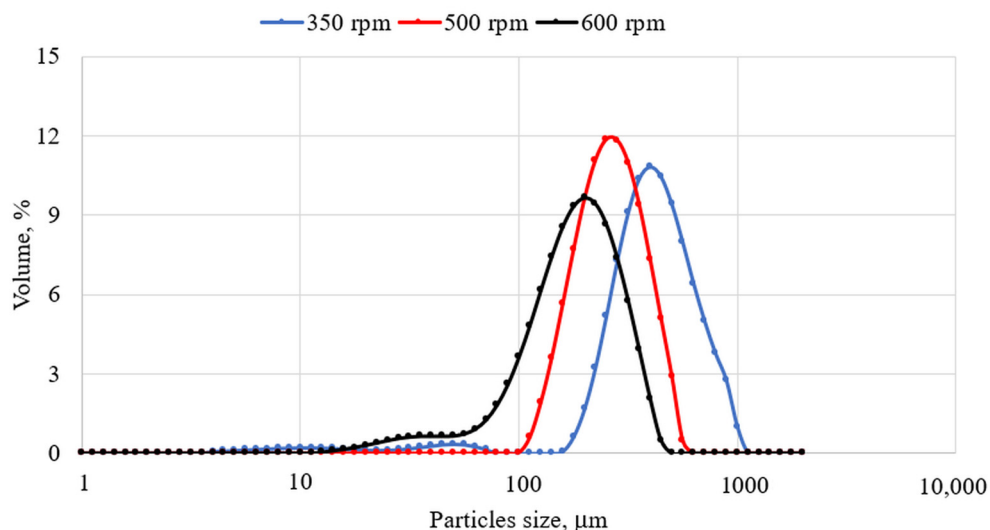


Figure 3. Size distributions of polymer particles prepared in the presence of $\text{Fe}_3\text{O}_4@\text{OA}$ depending on the stirring rate.

As mentioned above, the polymer particles synthesized in the presence of $\text{Fe}_3\text{O}_4@\text{OA}$ were characterized by a brownish color. This finding indicated that part of the magnetite particles underwent encapsulation inside the final polymer beads. However, the observed color of the polymer composite particles seemed to suggest that some of the magnetite particles could oxidize to maghemite ones during the polymerization and post-polymerization washing operations. The ICP OES analysis preceded by a previous mineralization of particle samples revealed that about 14% to 36% of the magnetite particles added to the monomer mixture were embedded in the final polymer beads. The percentage of $\text{Fe}_3\text{O}_4@\text{OA}$ embedded in the polymer microparticles increased with increasing amounts of magnetite nanoparticles being added to the monomer composition. However, at the same time, the percentage of $\text{Fe}_3\text{O}_4@\text{OA}$ particles encapsulated decreased in the same order.

Microphotographs taken using an optical stereomicroscope equipped with a digital camera showed that polymer particles that did not contain the $\text{Fe}_3\text{O}_4@\text{OA}$ additive differed in their transparency compared to those obtained in the presence of magnetite particles (Figure 4). They are also different from the polymer particles that were obtained based on the GMA-S-DVB composition diluted with the cyclohexanol/1-octanol mixture [55]. The

rather milky appearance of the polymer microparticles obtained using toluene indicated that this solvent acts not only as a diluent for the monomer composition, but also as a porogen for the polymer network of particles formed under the applied polymerization conditions [59]. This phenomenon probably resulted from the incompatibility of hydrophobic toluene molecules and polar glycidyl methacrylate molecules that were present in the monomer composition in the amount of 20 mol%. Furthermore, the microphotographs revealed that the polymer particles obtained in the presence of 0.05 and 0.1 wt.% $\text{Fe}_3\text{O}_4@\text{OA}$ contained microbubbles inside and appeared to resemble the multihollow morphology particles described by Du Prez et al. [39]. The number of microbubbles ('gigapores') in individual particles increased as the amount of $\text{Fe}_3\text{O}_4@\text{OA}$ in the monomer composition increased. Furthermore, the particles provided using 0.25 wt.% $\text{Fe}_3\text{O}_4@\text{OA}$ and more were characterized by a raspberry-like morphology like the particles described in refs. [60,61].

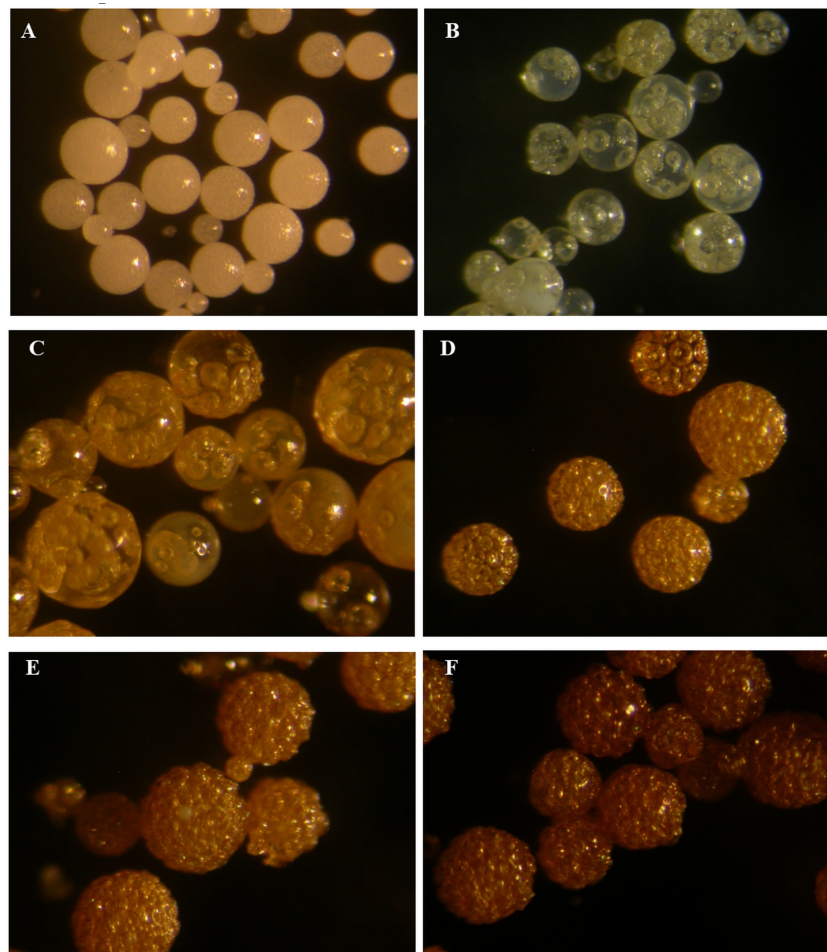


Figure 4. Microphotographs of GMA-based polymer microparticles prepared (A) without $\text{Fe}_3\text{O}_4@\text{OA}$ (**1a**) and with (B) 0.05 (**1b**), (C) 0.10 (**1c**), (D) 0.25 (**1d**), (E) 0.5 (**1e**), and (F) 0.75 wt.% $\text{Fe}_3\text{O}_4@\text{OA}$ (**1f**) additive.

More details on the morphology of the obtained particles were revealed after their examination using a SEM technique (Figure 5). The SEM images revealed the complex morphology of composite microparticles, which was initially concluded based on the optical microphotographs. Furthermore, the SEM images revealed that the surfaces of the composite microparticles are covered with numerous microcraters. The number of microcraters increased with an increasing concentration of $\text{Fe}_3\text{O}_4@\text{OA}$ particles in the monomer composition. Furthermore, the SEM analysis proved that the particles had an inhomogeneous morphology without the use of $\text{Fe}_3\text{O}_4@\text{OA}$ particles (Figure 5). The presence of numerous bubbles on the surface of the polymer particles appears to indicate this.

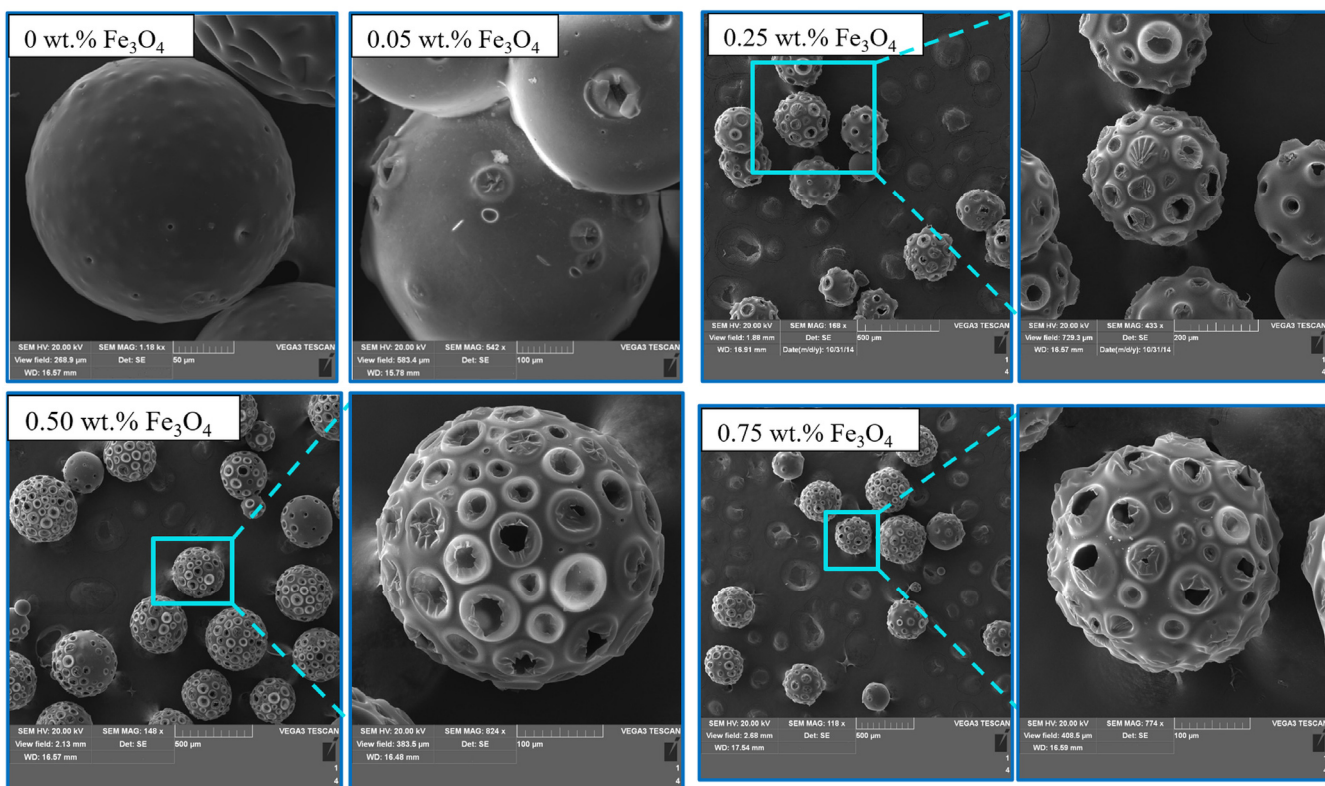


Figure 5. SEM images of GMA-based polymer microparticles prepared without $\text{Fe}_3\text{O}_4@\text{OA}$ (**1a**) and with 0.05 (**1b**), 0.25 (**1d**), 0.5 (**1e**), and 0.75 wt.% $\text{Fe}_3\text{O}_4@\text{OA}$ (**1f**) additive.

A SEM EDS analysis was performed for randomly selected craters on the surfaces of the composite beads (Figure 6). The presence of Fe atoms was detected at points 1 and 4, respectively, located inside and in the immediate vicinity of the examined crater. These findings demonstrate that $\text{Fe}_3\text{O}_4@\text{OA}$ particles play an active role in the formation of the raspberry-like or multi-hollow-like morphology of the composite microparticles produced. Hydrophobic nanoparticles and microparticles are capable of stabilizing water/oil emulsions during polymerization [62–65]. It is probable that, thanks to this feature, the hydrophobic nanoparticles of $\text{Fe}_3\text{O}_4@\text{OA}$ can easily disperse in the monomer phase and participate in the formation of ‘giga’ pores in the polymer composite microbeads provided as a consequence of polymerization.

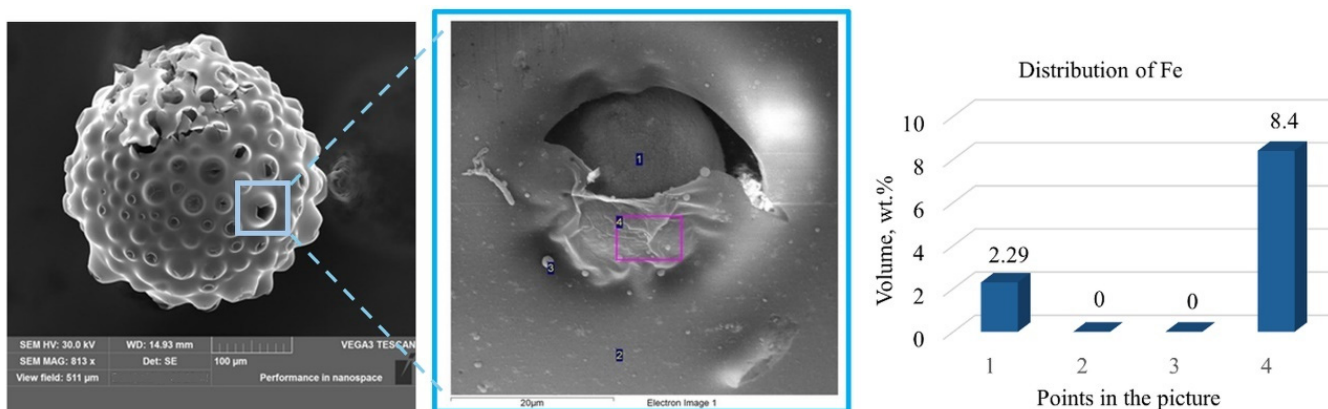


Figure 6. Distribution of iron atoms within composite microparticles obtained using 0.25 wt.% $\text{Fe}_3\text{O}_4@\text{OA}$ (**1d**).

An increase in the number of $\text{Fe}_3\text{O}_4@\text{OA}$ nanoparticles embedded in the resulting polymer composite particles should affect the magnetic properties of the latter. A very slight magnetic effect was only observed for the final microparticles that were obtained using 0.25 wt.% and more $\text{Fe}_3\text{O}_4@\text{OA}$ in relation to the monomers (Figure 7).

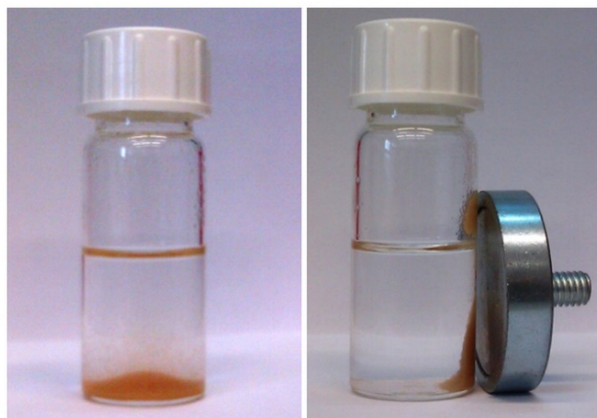


Figure 7. The performance of **1d** microparticles under the influence of a neodymium magnet.

The composite microparticles were also analyzed to assess the loading of epoxy groups introduced with GMA. The modified Jay method was applied [55]. The results obtained are presented in Table 2. When comparing these results with those previously obtained for GMA resins using the cyclohexanol/1-octanol mixture [55], it was concluded that, despite a certain ‘incompatibility’ in polarity between GMA and toluene molecules, the polymer composite particles obtained using toluene were characterized by epoxy group loadings comparable to those obtained previously [55].

Table 2. Characteristics of composite microparticles modified with PAMAM.

Polymerization Product	Epoxy Group Loading, mmol/	Modification Product	Nitrogen Content, wt.%	mmol/g	Epoxy Group Conversion, %
1a	1.33	-	-	-	-
1d	1.25	2d	4.99	3.56	36
1e	1.29	2e	5.74	4.10	41

The chemical structure of the composite particles was also studied by FTIR spectroscopy. The FTIR spectra of the provided particles were dominated by the absorption bands corresponding to the group characteristics of the monomers used for the polymerization (Figure 8). The adsorption bands at 1724 cm^{-1} ($\nu\text{C=O}$), between 1330 and 1050 (skeletal vibration of C–O–C) and at 908 and 825 cm^{-1} (epoxy ring stretching), can be attributed to GMA units. The bands observed in the ranges of 3080 to 2850 and 1600 to 1450 cm^{-1} confirm the presence of aliphatic and aromatic hydrocarbyl groups in the polymer structure. Due to the very low amount of Fe_3O_4 particles (below 0.1 wt.%) embedded in the final composite microparticles, the absorption band corresponding to the Fe–O–Fe skeletal vibrations in Fe_3O_4 (at approximately 570 cm^{-1}) was slightly visible in the spectra of composite particles as it was obscured by the much more intensive band of six-membered aromatic rings (Figure 8).

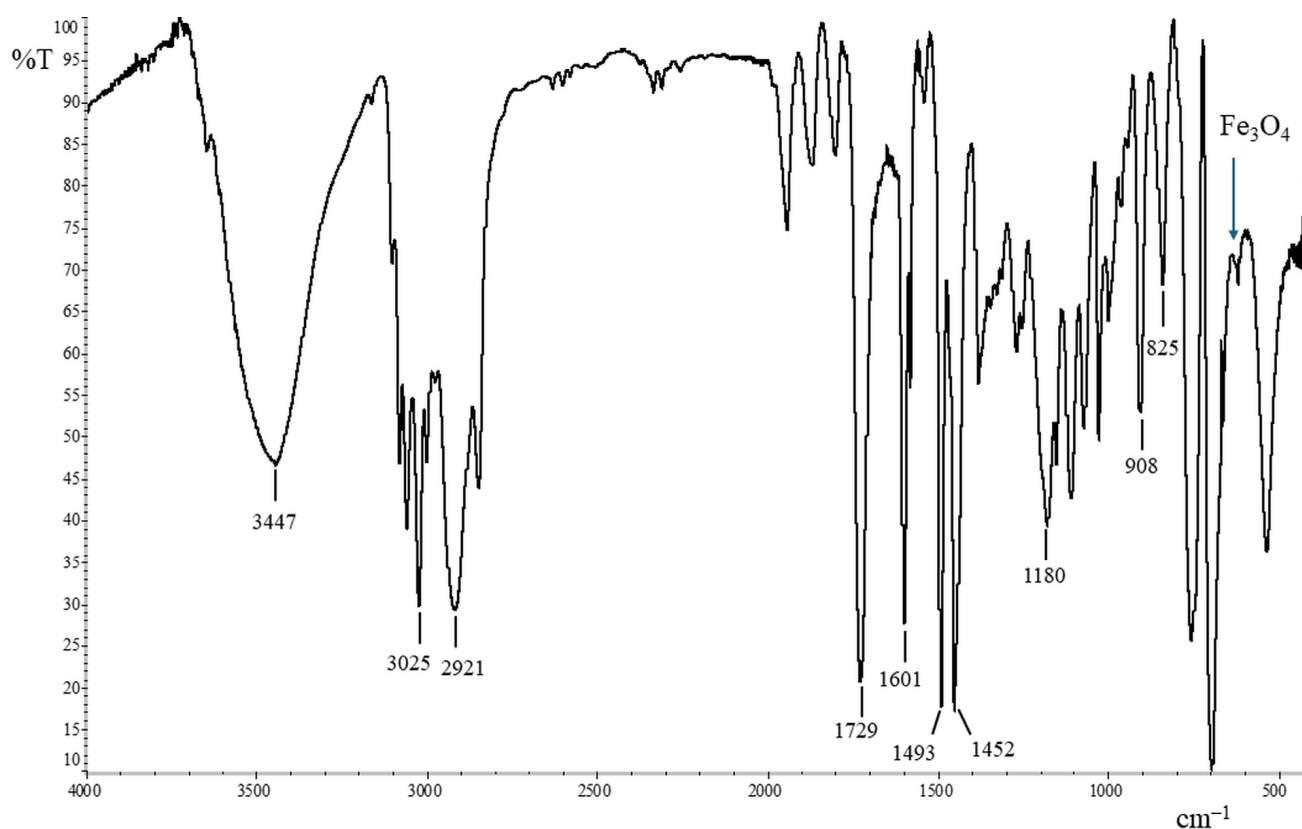


Figure 8. FTIR spectra of **1d**.

The swelling capacity of the obtained composite microparticles was also examined. The knowledge of this feature can be interesting from the point of view of further potential chemical modifications of the microparticles. Water, methanol, toluene, THF, DMF, and methylene chloride, as well as three mixed solvent systems, namely THF–water (1:1, (v:v)), toluene/methanol (1:1, (v:v)), and methylene chloride/methanol (3:1, 1:1, and 1:3 (v:v)), were used to perform the swelling experiments (Figure 9).

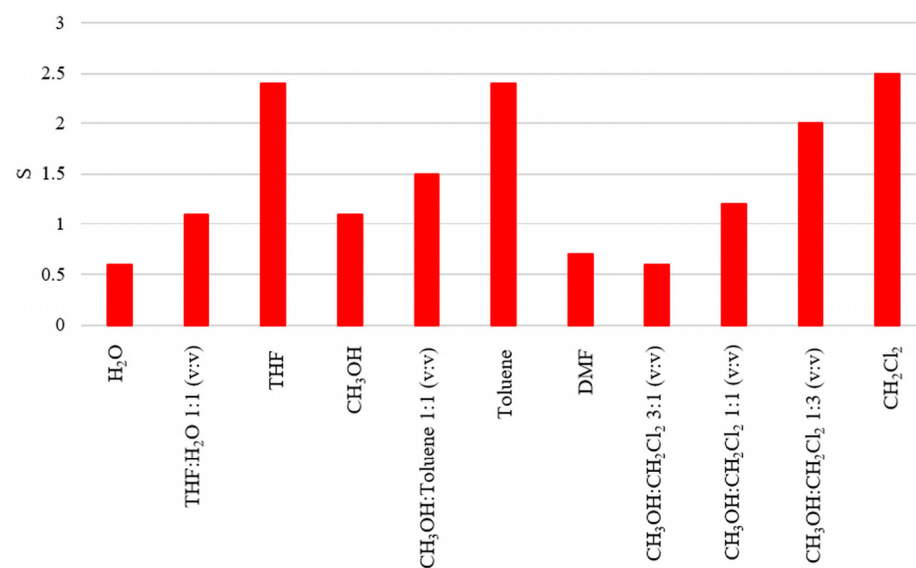


Figure 9. Increase in volume occupied by **1d** composite microspheres in different solvents.

The composite microparticles were clearly found to swell better in THF, toluene, methylene chloride, and the 1:3 *v:v* methanol/methylene chloride mixture than in water, methanol, and the 3:1 *v:v* methanol/methylene chloride mixture. The presence or an excess of a polar solvent did not favor the swelling of the microparticles. Generally, the swelling capacity of the composite microparticles was found to be quite like that observed for the GMA resins developed previously [55].

A thermogravimetric analysis was also performed for the selected polymerization product. Figure 10 presents the TGA and DTA curves recorded for the microparticles **1e**. No risk of thermal particle degradation was found under typical liquid phase reaction conditions. The slight weight loss observed below 300 °C could be related to the desorption of water and/or other solvents (toluene and acetone) absorbed on the surfaces of the microparticles. The particle decomposition clearly increased above 300 °C, reaching a maximum at about 390 °C.

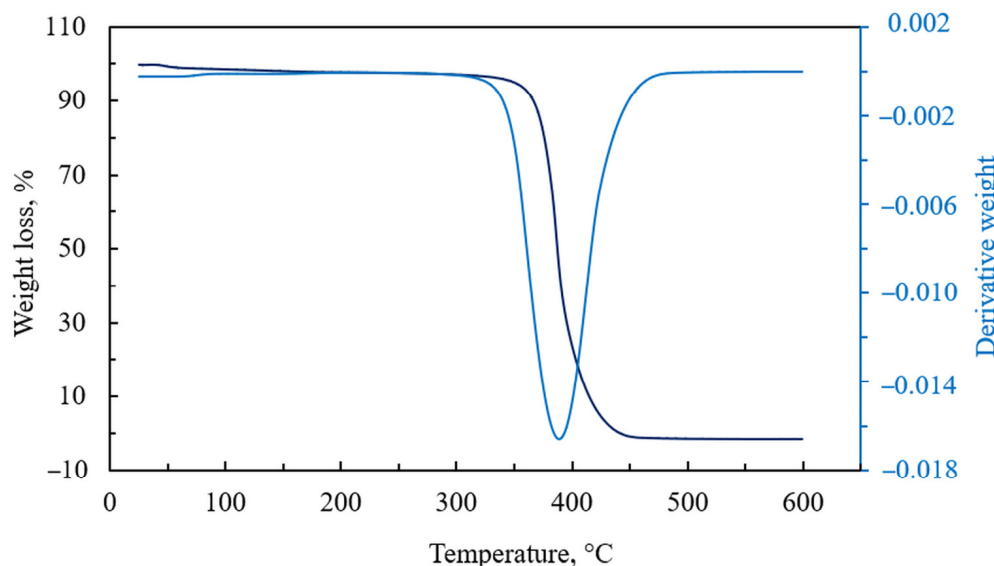


Figure 10. Thermogravimetric curves obtained for **1e**.

3.2. Attempts of Chemical Modification and Application of Composite Microparticles

As was mentioned in the Introduction Section, introducing epoxy groups into insoluble materials can be useful from the point of view of their subsequent chemical modifications. Therefore, the selected polymerization products (**1d** and **1e**), provided using 0.25 and 0.50 wt.% $\text{Fe}_3\text{O}_4@\text{OA}$, respectively, were modified according to Scheme 2 in the reaction with the zero-order PAMAM dendrimer. The modification was carried out similarly to that performed in the case of gel-type GMA-S-DVB terpolymers [66]. To prove the efficiency of the transformation of epoxy groups under the influence of primary amine groups in PAMAM, the FTIR spectra of the modified products were recorded and compared with the spectrum of epoxy-functionalized microparticles (Figure 11). A decrease in absorption in the range characteristic for the stretching vibration of the epoxide rings (908 and 825 cm^{-1}) and an increase in absorption in the range extending from 3600 to 3100 cm^{-1} corresponding to the stretching vibrations of the hydroxy and amine groups indicated the conversion of epoxy groups under the influence of PAMAN amine groups. Furthermore, the introduction of polyamineamide PAMAM units into the structure of the starting materials was demonstrated by the appearance of the new absorption bands at 1654 and 1546 cm^{-1} , which correspond to the vibrations of the amide units.

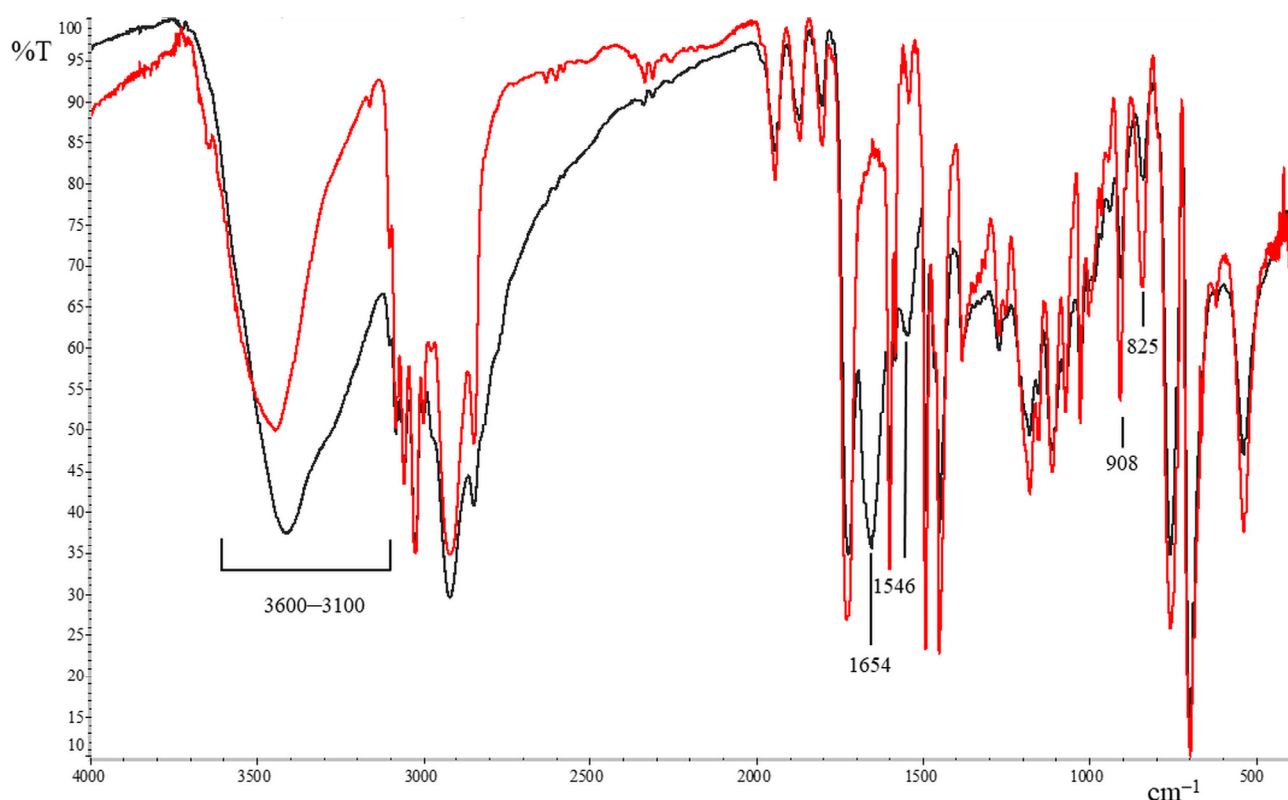
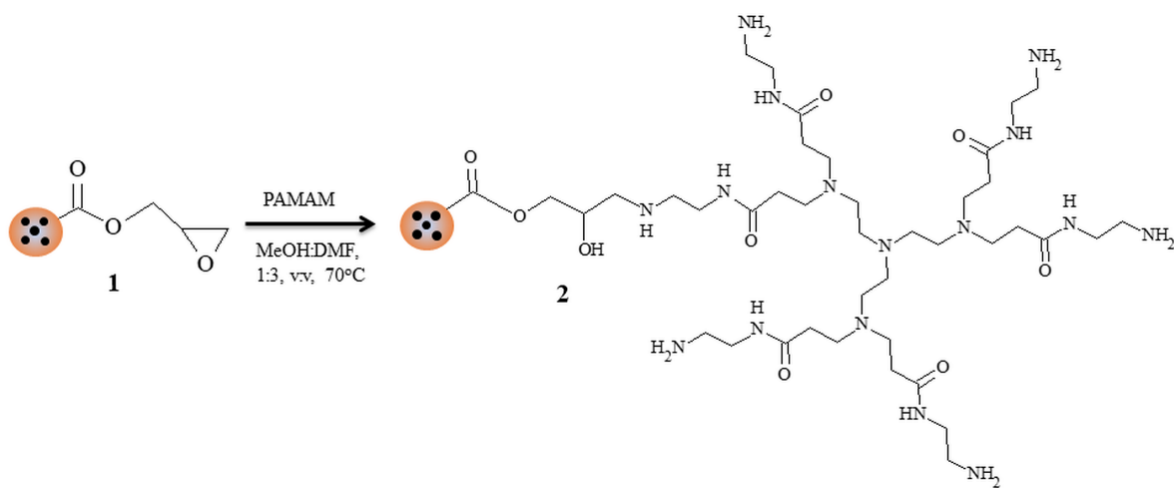


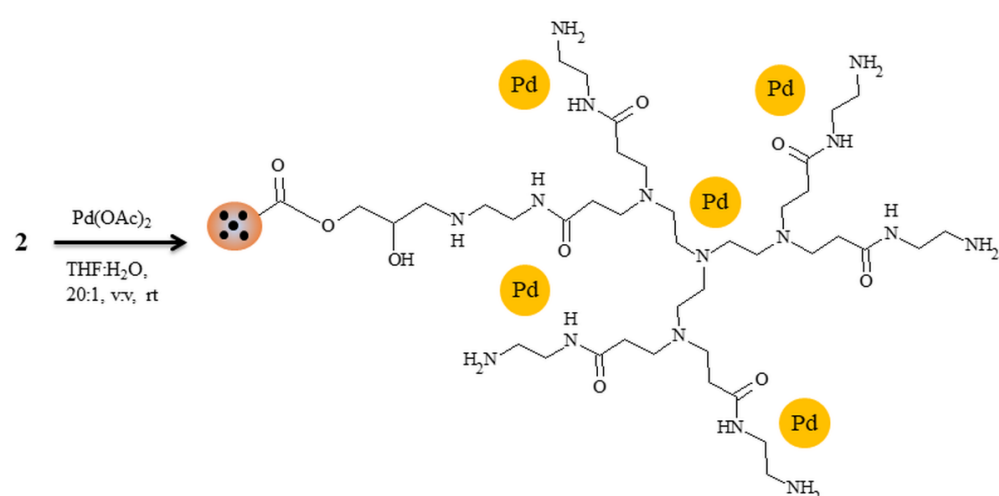
Figure 11. Comparison of FTIR spectra of **1d** and **2d**.

To assess the amino group loadings, the nitrogen contents in the modified particles were determined using the Kjeldahl method. Nitrogen percentages of 4.99–5.74 wt.% were found (Table 2). The values obtained pointed to approximately a 40% conversion of epoxy groups.



Scheme 2. Chemical modification of **1**.

The composite microparticles with immobilized PAMAM units (**2d** and **2e**) were then impregnated with the solutions of palladium(II) acetate in THF. Impregnation was performed at room temperature and lasted 24 h. An equivalent of Pd(II) ions in relation to the amine groups was applied to immobilize palladium(II) ions within the composite microparticles (Scheme 3).



Scheme 3. Immobilization of Pd(II) ions on **2**.

Only slight changes in color were observed for the resulting microparticles after impregnation (Figure 12). However, the occurrence of Pd(II) ion immobilization was proven by comparing the FTIR spectra of the microparticles recorded before and after impregnation (Figure 13). The comparison revealed an appearance of the new absorption bands in the spectra of the products at ~ 1560 and 1320 cm^{-1} . These findings could be attributed to vibrations within the C=O and C-O bonds, respectively, in the acetate ions [67]. The observation indicated that the Pd(II) ions underwent immobilization within the PAMAM-functionalized microparticles in the presence of acetate ions. However, the observed spectral changes did not point to which donor atoms are responsible for the immobilization of palladium(II) acetate. It is well known that Pd(II) ions generally form tetracoordinate complexes and can interact with various donor atoms. In the case of the polymer composite particles obtained based on glycidyl methacrylate modified with PAMAM and used as a support for Pd(CH₃COO)₂, theoretically, two groups of donor atoms (with oxygen and nitrogen atoms) can participate in coordination. However, the better donor properties in relation to Pd(II) ions seem to present nitrogen-type donors, particularly those located on amine groups. To underline the probable interactions, palladium species were located near these atoms/groups in the simplified scheme that presented a palladium-supported catalyst based on the obtained PAMAM-functionalized polymer composite particles.

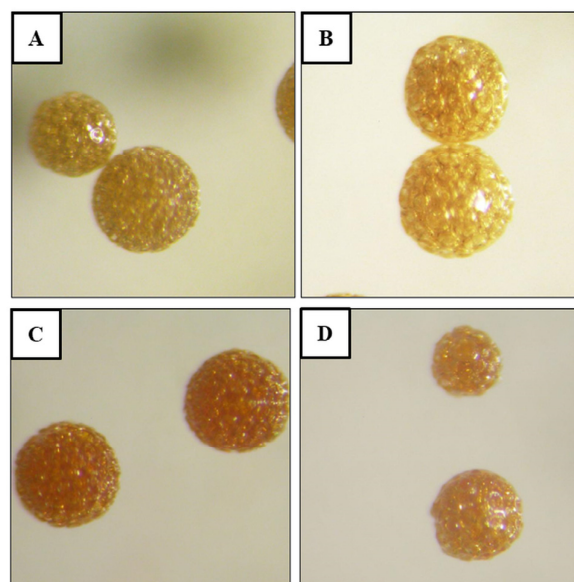


Figure 12. Comparison of microphotographs of **2d** (A), **2e** (B), **3d** (C), and **3e** (D).

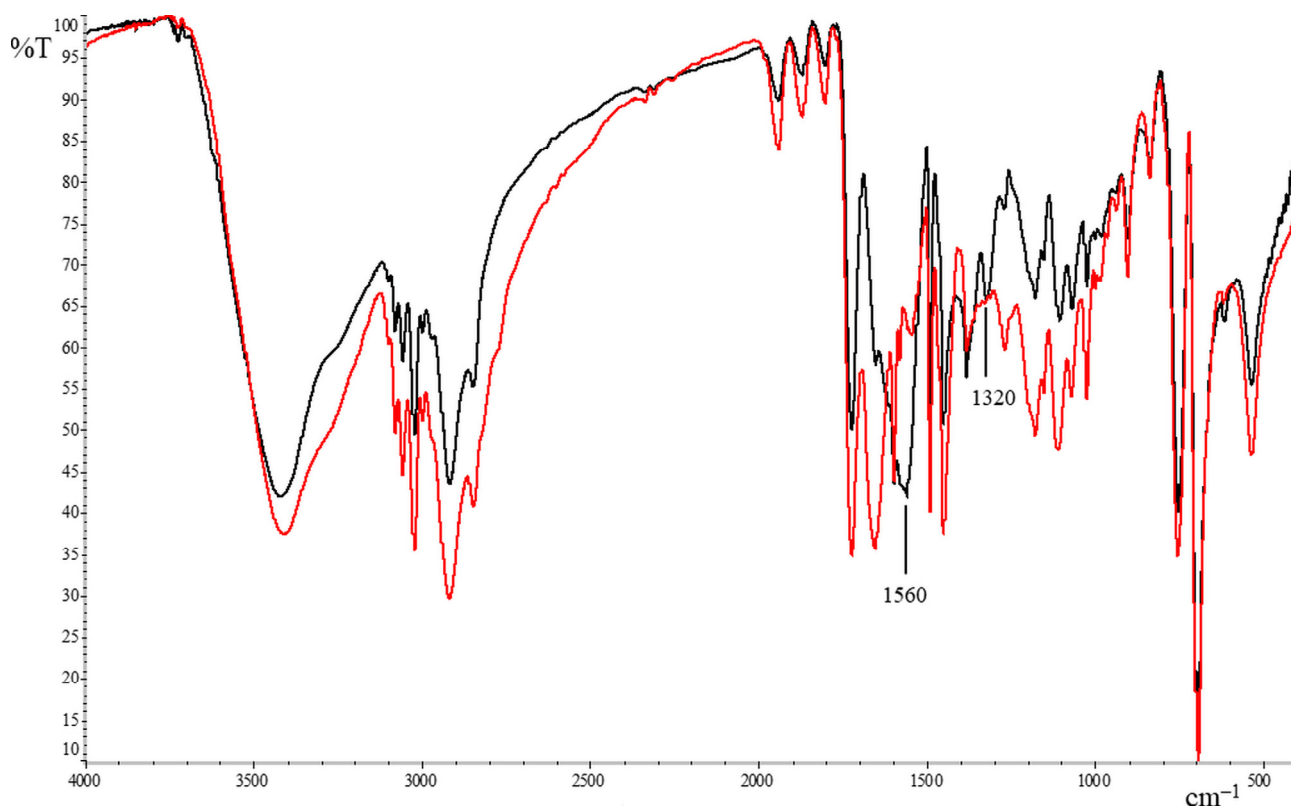
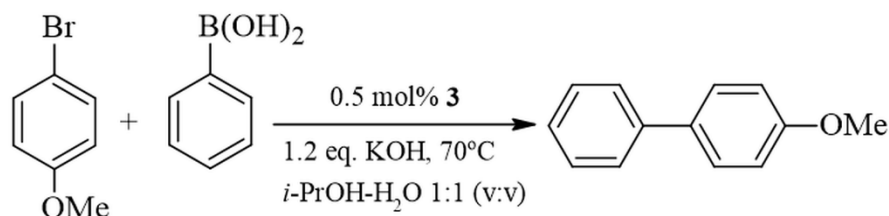


Figure 13. FTIR spectra of **2d** and **3d**.

ICP analyses of **3d** and **3e** were also performed. Impregnation products were found to contain 8.7 and 11.4 wt.% immobilized Pd(II) ions (0.81 and 1.07 mmol of Pd per gram), respectively.

As is well known, palladium plays a crucial role in catalyzing different coupling reactions that deliver important products, for example, for the pharmaceutical [68–71] and materials industries [69,72,73]. Numerous soluble and insoluble precursors were previously applied as a source of Pd(0) species that are responsible for activating substrates in these reactions. Among them, different modified polymeric, inorganic, and composite materials, including materials composed of magnetic nanoparticles, can be found [34,74–78]. Therefore, the use of developed composite microparticles as a source of catalytically active palladium species appeared to be interesting. The Suzuki coupling observed between 4-bromoanisole and phenylboronic acid was chosen as a model reaction to carry out the catalytic experiments in the presence of selected materials (Scheme 4). Catalytic experiments were carried out at 70 °C using a 1.2-fold molar excess of phenylboronic acid PhB(OH)₂ and **3d** or **3e** in the amount corresponding to 0.5 mol% Pd. The mixture of *i*-PrOH/H₂O (1:1; *v*:*v*) was applied as the reaction medium. Gas chromatography was used to determine the conversion of 4-bromoanisole after the assumed time periods.



Scheme 4. Suzuki reaction used for catalytic examination.

The catalysts used in the experiments were found to allow 4-bromoanisole to be quantitatively converted in approximately 60 min under the applied reaction conditions, al-

though the coupling reactions kicked off with some delay (Figure 14). The experiments also showed that **3e** with higher palladium (1.07 mmol/g) and magnetite loadings (0.068 wt.% Fe determined by ICP) turned out to be slightly more active than **3d** (0.81 mmol Pd(II)/g; 0.048 wt.% Fe from ICP analysis). Furthermore, it was concluded that the catalytic activities of **3d** and **3e** were considerably higher compared to the activity of the palladium catalyst based on gel-type polymer particles that were prepared without the addition of magnetite nanoparticles [65]. The presence of magnetite nanoparticles embedded within a gel-type polymer matrix can improve the dispersion of Pd(0) species on the surface and inside of a polymeric support, making them more active in the Suzuki reaction. The observed induction periods can result from the need for a preliminary transformation of inactive catalytically immobilized Pd(II) ions into active Pd(0) species, which occurs not only on the inert surface but also inside gel-type microbeads. Furthermore, the solvent used as the reaction medium does not favor the swelling of the polymer composite microparticles used as the palladium support, and more time is required for substrates to penetrate inside the polymer beads and interact with catalytic centers; however, the solvent that was used facilitates Suzuki coupling.

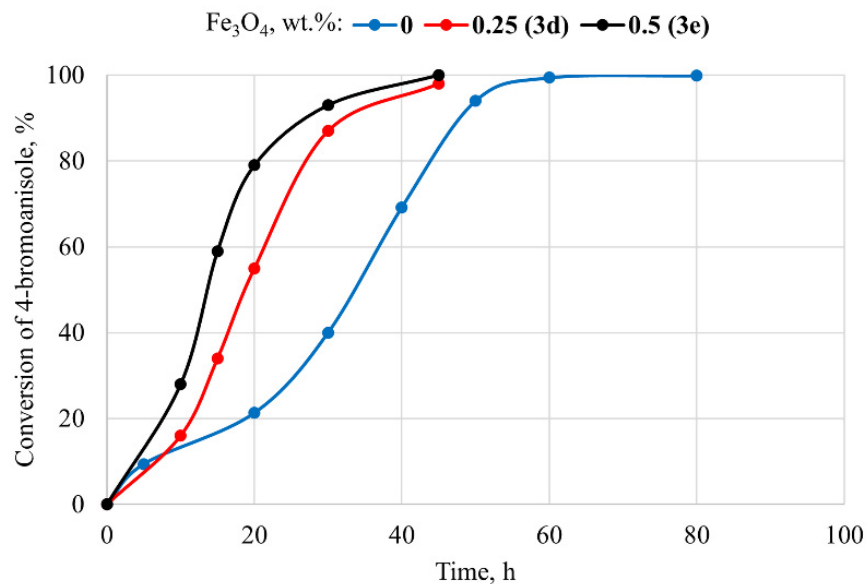


Figure 14. Changes in the conversion of 4-bromoanisole as a function of time; 0.5 mol% **3**, 70 °C.

Next, **3e** was used in the recycling experiments, and the results are presented in Figure 15. It was found that the catalyst induction time increased with each catalyst reuse. However, the activity remained at a high level even when **3e** was reused in the seventh cycle. The approximately 86% conversion of 4-bromoanisole in the reaction with boronic acids could then be obtained after 180 min.

The decrease in the catalytic activity observed in the recycling experiments was probably due to the partial release of palladium nanoparticles from the support to the reaction mixture, as well as due to the deposition of larger, less active palladium black particles on the surfaces of the composite particles while the coupling occurs. The last factor was probably responsible for prolonging the induction times when **3e** was recovered and reused. Palladium leaching and changes in the form of palladium(0) species were not investigated in this work in detail, although it is well known that the problems mentioned above are often encountered in palladium-catalyzed coupling reactions [79]. The problems of decreasing the catalytic activity during catalyst recovery and recycling were discussed in our previous works describing the possibility of using gel-type amine-functionalized polymer particles with immobilized palladium(II) acetate as catalysts for S-M reactions [56,80].

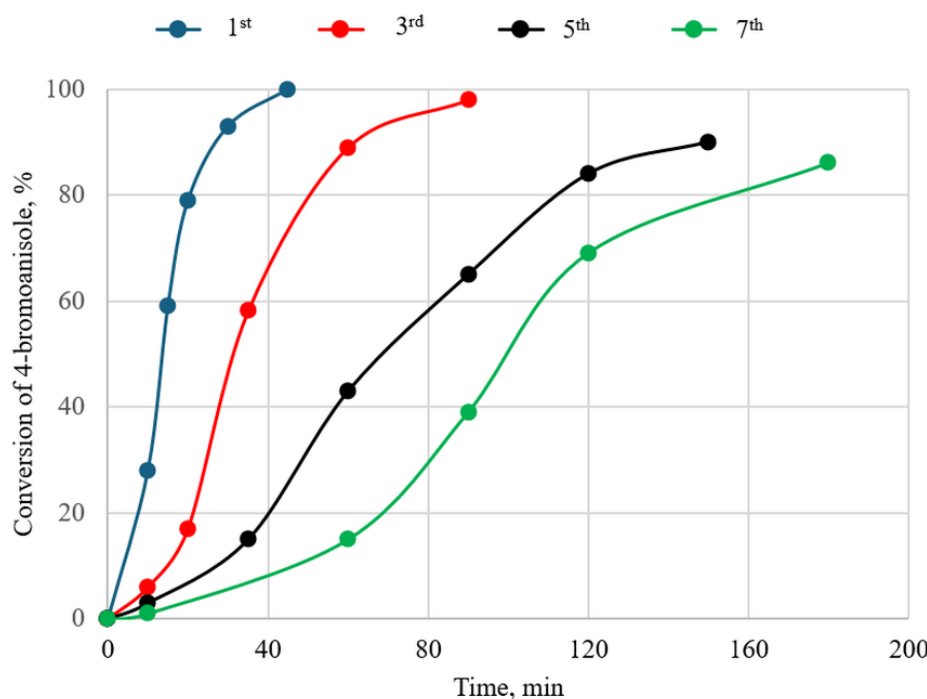
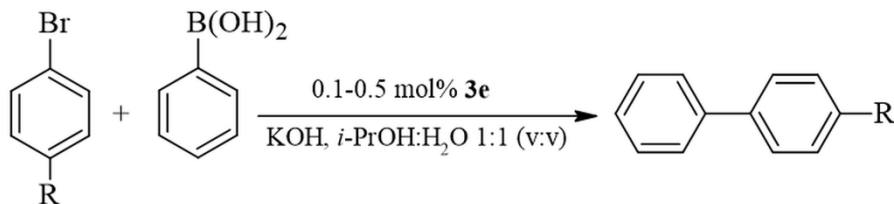


Figure 15. Conversion of 4-bromoanisole as a function of time at catalyst recycling attempts; 0.5 mol% **3e**, 60 °C.

Finally, the catalyst concentration and reaction temperature were found to have effects on the conversion of 4-bromoanisole in the reaction with phenylboronic acid (Table 3, entries 1–5). It was found that the coupling occurred efficiently even in the case where **3e** was used in the amount of 0.1 mol% Pd (98% conversion after 150 min, Table 3, entry 1) and when the reaction temperature was lowered to 25 °C (88% conversion after 360 min, Table 3, entry 4). Furthermore, **3e** was also examined as a catalyst in the S-M reactions between phenylboronic acid and several other aryl bromides (Table 3, entries 6–9). High conversions of the appropriate aryl bromides were obtained in 20–90 min in these cases. The lowest reactivity in the reaction with phenylboronic acid was found for 4-bromofluorobenzene.

Table 3. Results of the Suzuki–Miyaura cross-coupling reactions.



Entry	R	T °C	Catalyst 3e , mol%	Time, min	Conversion of ArBr, %
1	OCH ₃	70	0.1	150	98
2	OCH ₃	70	0.25	60	100
3	OCH ₃	70	0.5	45	100
4	OCH ₃	25	0.5	360	88
5	OCH ₃	50	0.5	120	96
6	H	70	0.5	20	100
7	CHO	70	0.5	10	100
8	Naphthyl	70	0.5	30	97
9	F	70	0.5	90	96

4. Conclusions

The addition of $\text{Fe}_3\text{O}_4@\text{OA}$ to the composition of monomers consisting of glycidyl methacrylate (GMA), styrene (S), divinylbenzene (DVB), benzoyl peroxide (an initiator), and toluene (a diluent) resulted in obtaining polymer microparticles that had the unique multi-hollow or raspberry-like morphology and composite character in suspension polymerization. Hydrophobized MNPs added to the monomer composition turned out to be responsible for the stabilization of water droplets in the organic phase and the shaping of the multi-hollow morphology of the provided composite particles during the polymerization. The number of microbubbles formed by stabilized water droplets within the produced polymer microparticles increased with increasing amounts of $\text{Fe}_3\text{O}_4@\text{OA}$ nanoparticles added, resulting in their surfaces being covered with numerous microcraters that shaped their final raspberry-like morphology. The magnetite nanoparticles used for the polymerization underwent partial embedding within the formed polymer network, providing the composite nature for the polymer microparticles. However, the amount of magnetic nanoparticles encapsulated within the polymer composite microparticles did not exceed 0.1 wt.%; thus, the resulting particles showed only very slight magnetic properties that were insufficient for magnetic separation. The use of divinylbenzene (a crosslinking monomer) in an amount of 3 mol% and styrene in an amount of 77 mol%, as well as the dilution of the monomer mixture with toluene, resulted in the formation of gel-type microparticles with good swelling capacity in THF, toluene, methylene chloride, and the mixture of 1:3 v:v methanol/methylene chloride. Introducing epoxy groups into the polymer network with glycidyl methacrylate molecules allowed the further modification of the composite particles in the reaction with PAMAM-type polymidoamine followed by the immobilization of palladium(II) ions within the microparticles. The materials obtained were thus successfully used as sources of Pd(0) particles that are active in coupling reactions between phenylboronic acid and various aryl bromides. It was concluded that the activity of the catalysts based on the polymer composite microparticles was clearly higher than that of the catalyst based on the polymeric support with the pure gel-type nature. The presence of inorganic nanoparticles embedded within a gel-type polymer matrix appeared to improve the dispersion of Pd(0) species on the surface and inside of the polymer composite supports, making them more active in the Suzuki reaction.

Author Contributions: Conceptualization, W.B. and A.B.; methodology, W.B. and A.B.; formal analysis and investigation, S.F., K.B. and A.B.; data curation, W.B. and A.B.; writing—original draft preparation, W.B. and A.B.; writing—review and editing, W.B. and A.B.; visualization, A.B.; supervision, W.B. All authors have read and agreed to the published version of the manuscript.

Funding: This research received no external funding.

Data Availability Statement: All data are given in the paper.

Conflicts of Interest: The authors declare no conflict of interest.

References

- Yudin, A.K. *Aziridines and Epoxides in Organic Synthesis*; Wiley-VCH: Weinheim, Germany, 2008.
- Xiao, J.; Lu, Q.; Cong, H.; Shen, Y.; Yu, B. Microporous poly(glycidyl methacrylate-co-ethylene glycol dimethyl acrylate) microspheres: Synthesis, functionalization, and applications. *Polym. Chem.* **2021**, *12*, 6050–6070. [[CrossRef](#)]
- Vera, M.; Fodor, C.; Garcia, Y.; Pereira, E.; Loos, K.; Rivas, B.L. Multienzymatic immobilization of laccases on polymeric microspheres: A strategy to expand the maximum catalytic, Efficiency. *J. Appl. Polym. Sci.* **2020**, *137*, 49562. [[CrossRef](#)]
- Vasiliu, S.; Lungan, M.-A.; Racovita, S.; Popa, M. Porous microparticles based on methacrylic copolymers and gellan as drug delivery systems. *Polym. Int.* **2020**, *69*, 1066–1080. [[CrossRef](#)]
- Akbari, K.; Moghadam, P.N.; Behrouzi, M.; Fareghi, A.R. Synthesis of three-dimensional hydrogels based on poly(glycidyl methacrylate-alt-maleic anhydride): Characterization and study of furosemide drug release. *Arab. J. Chem.* **2020**, *13*, 8723–8733. [[CrossRef](#)]
- Horák, D.; Švec, F.; Bleha, M.; Kálal, J. Reactive polymers, XXXV. The effect of polymerization conditions on the specific surface area of macroporous copolymers from glycidylmethacrylate-ethylenedimethacrylate. *Angew. Makromol. Chem.* **1981**, *95*, 109–115. [[CrossRef](#)]

7. Nastasović, A.; Marković, B.; Suručić, L.; Onjia, A. Methacrylate-based polymeric sorbents for recovery of metals from aqueous solutions. *Metals* **2022**, *12*, 814. [[CrossRef](#)]
8. Drake, R.; Dunn, R.; Sherrington, D.C.; Thomson, S.J. Polymethacrylate and polystyrene-based resin-supported Pt catalysts in room temperature, solvent-less, oct-l-ene hydrosilylations using trichlorosilane and methyldichlorosilane. *J. Molec. Catal. A Chem.* **2001**, *177*, 49–69. [[CrossRef](#)]
9. Bukowska, A.; Bukowski, W.; Bester, K.; Hus, K. Polymer supported copper(II) amine-imine complexes in the C-N and A³ coupling reactions. *Appl. Organometal. Chem.* **2017**, *31*, 3847. [[CrossRef](#)]
10. Fofana, M.; Kuma, M.S. Use of a magnetic fluid-based process for coal separations. *Miner. Met. Rev.* **1997**, *38*, 35–40.
11. Hatami, M.; Mohammadi-Rezaei, S.; Tahari, M.; Jing, D. Recent developments in magneto-hydrodynamic Fe₃O₄ nanofluids for different molecular applications: A review study. *J. Molec. Liq.* **2018**, *250*, 244–258. [[CrossRef](#)]
12. Khollam, Y.B.; Dhage, S.R.; Potdar, H.S.; Deshpande, S.B.; Bakare, P.P.; Kulkarni, S.D.; Date, S.K. Microwave hydrothermal preparation of submicron-sized spherical magnetite (Fe₃O₄) powders. *J. Magn. Magn. Mater.* **2002**, *56*, 571–577. [[CrossRef](#)]
13. Ali, A.; Shah, T.; Ullah, R.; Zhou, P.; Guo, M.; Ovais, M.; Tan, Z.; Rui, Y. Review on recent progress in magnetic nanoparticles: Synthesis, characterization, and diverse applications. *Front. Chem.* **2021**, *9*, 629054. [[CrossRef](#)] [[PubMed](#)]
14. Soltys, L.; Olkhovyy, O.; Tatarchuk, T.; Naushad, M. Green synthesis of metal and metal oxide nanoparticles: Principles of green chemistry and raw materials. *Magnetochemistry* **2021**, *7*, 145. [[CrossRef](#)]
15. Gambhir, R.P.; Rohiwal, S.S.; Tiwari, A.P. Multifunctional surface functionalized magnetic iron oxide nanoparticles for biomedical applications: A review. *Appl. Surf. Sci. Adv.* **2022**, *11*, 100303. [[CrossRef](#)]
16. Ansari, K.; Ahmad, R.; Tanweer, M.S.; Azam, I. Magnetic iron oxide nanoparticles as a tool for the advancement of biomedical and environmental application: A review. *Biomed. Mater. Devices* **2023**, *2*, 139–157. [[CrossRef](#)]
17. Fatmawati, T.; Shiddiq, M.; Armynah, B.; Tahir, D. Synthesis methods of Fe₃O₄ nanoparticles for biomedical applications. *Chem. Eng. Technol.* **2023**, *46*, 2356–2366. [[CrossRef](#)]
18. Iota, M.A.; Cursaru, L.M.; Schiopu, A.G.; Tudor, I.A.; Motoc, A.M.; Piticescu, R.M. Fe₃O₄ Core–shell nanostructures with anticancer and antibacterial properties: A Mini-review. *Processes* **2023**, *11*, 1882. [[CrossRef](#)]
19. Wang, Y.; Liu, X.; Ma, S.; He, X.; Guo, C.; Liang, Z.; Hu, Y.; Wei, Y.; Lian, X.; Huang, D. Progress in cancer therapy with functionalized Fe₃O₄ nanomaterials. *Front. Mater. Sci.* **2023**, *17*, 230658. [[CrossRef](#)]
20. Lu, A.H.; Salabas, E.L.; Schüth, F. Magnetic nanoparticles: Synthesis, protection, functionalization, and application. *Angew. Chem. Int. Ed.* **2007**, *46*, 1222–1244. [[CrossRef](#)]
21. Laurent, S.; Forge, D.; Port, M.; Roch, A.; Robic, C.; Elst, L.V.; Muller, R.N. Magnetic iron oxide nanoparticles: Synthesis, stabilization, vectorization, physicochemical characterizations, and biological applications. *Chem. Rev.* **2008**, *108*, 2064–2110. [[CrossRef](#)] [[PubMed](#)]
22. Nguyen, M.D.; Tran, H.V.; Xu, S.; Lee, T.R. Fe₃O₄ Nanoparticles: Structures, synthesis, magnetic properties, surface functionalization, and emerging applications. *Appl. Sci.* **2021**, *11*, 11301. [[CrossRef](#)] [[PubMed](#)]
23. Morais, P.C.; Garg, V.K.; Oliveira, A.C.; Silva, L.P.; Silva, R.B.; Silva, A.M.L.; Lima, E.C.D. Synthesis and characterization of size-controlled cobalt-ferrite-based ionic ferrofluids. *J. Magn. Magn. Mat.* **2001**, *225*, 37–40. [[CrossRef](#)]
24. Shen, L.; Li, B.; Qiao, Y. Fe₃O₄ Nanoparticles in targeted drug/gene delivery systems. *Materials* **2018**, *11*, 324. [[CrossRef](#)] [[PubMed](#)]
25. Zhang, X.; Niu, H.; Pan, Y.; Shi, Y.; Cai, Y. Chitosan-coated octadecyl-functionalized magnetite nanoparticles: Preparation and application in extraction of trace pollutants from environmental water samples. *Anal. Chem.* **2010**, *82*, 2363–2371. [[CrossRef](#)] [[PubMed](#)]
26. Xu, S.; Yan, Y.; Shuang, C.; Zhou, Q.; Ji, R.; Li, A. Biological magnetic ion exchange resin on advanced treatment of synthetic wastewater. *Bioresour. Technol.* **2023**, *372*, 128613. [[CrossRef](#)] [[PubMed](#)]
27. Sun, S.; Meng, X.; Lv, Z.; Jiang, T.; Liang, Q.; Shi, L.; Feng, J. Research progress on the removal of pesticides in water by Fe₃O₄-based adsorbents in the past decade: A review. *Arab. J. Chem.* **2024**, *17*, 105405. [[CrossRef](#)]
28. Dong, X.; Zheng, Y.; Huang, Y.; Chen, X.; Jing, X. Synthesis and characterization of multifunctional poly(glycidyl methacrylate) microspheres and their use in cell separation. *Anal. Biochem.* **2010**, *405*, 207–212. [[CrossRef](#)] [[PubMed](#)]
29. Lin, L.S.; Cong, Z.X.; Cao, J.B.; Ke, K.M.; Peng, Q.L.; Gao, J.; Yang, H.H.; Liu, G.; Chen, X. Multifunctional Fe₃O₄@polydopamine core&shell nanocomposites for intracellular mRNA detection and imaging-guided photothermal therapy. *ACS Nano* **2014**, *8*, 3876–3883.
30. Wu, W.; Wu, Z.; Yu, T.; Jiang, C.; Kim, W.S. Recent progress on magnetic iron oxide nanoparticles: Synthesis, surface functional strategies and biomedical applications. *Sci. Technol. Adv. Mater.* **2015**, *16*, 023501. [[CrossRef](#)]
31. Han, M.; Li, X.; Wang, X.; Liu, D.; Fu, S.; Xu, W.; Li, W.; Zhang, H. Preparation of polyhydroxyalkanoate-based magnetic microspheres for carbonyl reductase purification and immobilization. *Int. J. Biol. Macromol.* **2023**, *253*, 126814. [[CrossRef](#)]
32. Wan, G.Z.; Ma, X.H.; Jin, L.; Chen, J. Fabrication of a magnetic porous organic polymer for α-glucosidase, immobilization and its application in inhibitor screening. *Langmuir* **2023**, *39*, 5239–5249. [[CrossRef](#)]
33. Zhu, Y.; Stubbs, L.P.; Ho, F.; Liu, R.; Ship, C.P.; Maguire, J.A.; Hosmane, N.S. Magnetic nanocomposites: A new perspective in catalysis. *ChemCatChem* **2010**, *2*, 365–374. [[CrossRef](#)]
34. Sharma, R.K.; Dutta, S.; Sharma, S.; Zboril, R.; Varma, R.S.; Gawande, M.B. Fe₃O₄ (iron oxide)-supported nanocatalysts: Synthesis, characterization and applications in coupling reactions. *Green Chem.* **2016**, *18*, 3184–3209. [[CrossRef](#)]

35. Liu, R.; Guo, Y.; Odusote, G.; Qu, F.; Priestley, R.D. Core-shell Fe₃O₄ polydopamine nanoparticles serve multipurpose as drug carrier, catalyst support and carbon adsorbent. *ACS Appl. Mater. Interfaces* **2013**, *5*, 9167–9171. [CrossRef]
36. Horák, D.; Babic, M.; Macková, H.; Benes, M.J. Preparation and properties of magnetic nano- and microsized particles for biological and environmental separations. *J. Sep. Sci.* **2007**, *30*, 1751–1772. [CrossRef] [PubMed]
37. Wahajuddin, N.; Arora, S. Superparamagnetic iron oxide nanoparticles: Magnetic nanoplatforms as drug carriers. *Int. J. Nanomed.* **2012**, *7*, 3445–3471. [CrossRef]
38. Bustamante-Torres, M.; Romero-Fierro, D.; Estrella-Nuñez, J.; Arcentales-Vera, B.; Chichande-Proaño, E.; Bucio, E. Polymeric Composite of Magnetite Iron Oxide Nanoparticles and Their Application in Biomedicine: A Review. *Polymers* **2022**, *14*, 752. [CrossRef]
39. Gokmen, M.T.; Du Prez, F.E. Porous polymer particles—A comprehensive guide to synthesis, characterization, functionalization and applications. *Prog. Polym. Sci.* **2012**, *37*, 365–405. [CrossRef]
40. Wang, C.; Yan, J.; Cui, X.; Cong, D.; Wang, H. Preparation and characterization of magnetic hollow PMMA nanospheres via in situ emulsion polymerization. *Colloids Surf. A Physicochem. Eng. Asp.* **2010**, *363*, 71–77. [CrossRef]
41. Xu, S.; Ma, W.F.; You, L.J.; Li, J.M.; Guo, J.; Hu, J.J.; Wang, C.C. Toward designer magnetite/polystyrene colloidal composite microspheres with controllable nanostructures and desirable surface functionalities. *Langmuir* **2012**, *28*, 3271–3278. [CrossRef]
42. Xu, H.; Cui, L.; Tong, N.; Gu, H. Development of high magnetization Fe₃O₄/polystyrene/silica nanospheres via combined miniemulsion/emulsion polymerization. *J. Am. Chem. Soc.* **2006**, *128*, 15582–15583. [CrossRef] [PubMed]
43. Darwish, M.S.A.; Peuker, U.; Kunz, U. Bi-layer polymer-magnetite core/shell particles: Synthesis and characterization. *J. Mater. Sci.* **2011**, *46*, 2123–2134. [CrossRef]
44. Hu, J.; Chen, M.; Wu, L. Organic-inorganic nanocomposites synthesized via miniemulsion polymerization. *Polym. Chem.* **2011**, *2*, 760–772. [CrossRef]
45. Ma, Z.; Guan, Y.; Liu, H. Synthesis and characterization of micron-sized monodisperse superparamagnetic polymer particles with amino groups. *J. Polym. Sci. Part A Polym. Chem.* **2005**, *43*, 3433–3439. [CrossRef]
46. Zhang, J.; Yu, D.; Chen, W.; Xie, Y.; Wan, W.; Liang, H.; Min, C. Preparation of poly(styrene-glycidylmethacrylate)/Fe₃O₄ composite microsphere with high magnetite contents. *J. Magn. Magn. Mater.* **2009**, *321*, 572–577. [CrossRef]
47. Wang, C.; Zhang, C.; Li, Y.; Chen, Y.; Tong, Z. Facile fabrication of nanocomposite microspheres with polymer cores and magnetic shells by Pickering suspension polymerization. *React. Funct. Polym.* **2009**, *69*, 750–754. [CrossRef]
48. Wang, L.; Tai, Y.; Gao, J.; Amer, W.A.; Ding, W.; Yu, H. Synthesis of Fe₃O₄@poly(methylmethacrylate-co-divinylbenzene) magnetic porous microspheres and their application in the separation of phenol from aqueous solutions. *J. Colloid Interface Sci.* **2011**, *360*, 731–738.
49. Aksimentyeva, O.I.; Savchyn, V.P.; Dyakonov, V.P.; Piechota, S.; Horbenko, Y.Y.; Opainych, I.Y.; Demchenko, P.Y.; Popov, A.; Szymczak, H. Modification of Polymer-Magnetic Nanoparticles by Luminescent and Conducting Substances. *Mol. Crys. Liq. Cryst.* **2014**, *590*, 35–42. [CrossRef]
50. Lu, M.; Bai, S.; Yang, K.; Sun, Y. Synthesis and characterization of magnetic polymer microspheres with a core-shell structure. *China Particulol.* **2007**, *5*, 180–185. [CrossRef]
51. Bukowska, A.; Bukowski, W.; Hus, K.; Depciuch, J.; Parlińska-Wojtan, M. Synthesis and characterization of new functionalized polymer-Fe₃O₄ nanocomposite particles. *Express Polym. Lett.* **2017**, *11*, 2–13. [CrossRef]
52. Wang, L.; Yang, T.; Yang, J.; Li, Q.; Hao, D.; Yang, J.; Ma, G. *In situ* magnetization technique for synthesis of magnetic polymer microspheres. *Powder Technol.* **2013**, *235*, 1017–1024. [CrossRef]
53. Rabelo, D.; Lima, E.C.D.; Reis, A.C.; Nunes, W.C.; Novak, M.A.; Garg, V.K.; Oliveira, A.C.; Morais, P.C. Preparation of Magnetite Nanoparticles in Mesoporous Copolymer Template. *Nano Lett.* **2001**, *1*, 105–108. [CrossRef]
54. Liu, H.; Liu, X.; Xing, J.; Guan, Y.; Ma, Z.; Shan, G.; Yang, C. Preparation and characterization of superparamagnetic functional polymeric microparticles. *China Particulol.* **2003**, *1*, 76–79. [CrossRef]
55. Bukowska, A.; Bukowski, W.; Noworól, J. Three-component terpolymers of glycidyl methacrylate with good swelling characteristics. *J. Appl. Polym. Sci.* **2007**, *106*, 3800–3807. [CrossRef]
56. Bester, K.; Bukowska, A.; Bukowski, W. Palladium catalysts supported on amine-functionalized glycidyl methacrylate gel type terpolymers. Synthesis, characteristics and study of catalytic activity in Suzuki–Miyaura reactions. *J. Molec. Catal. A Chem.* **2013**, *378*, 124–134. [CrossRef]
57. Duraczyńska, D.; Serwicka, E.M.; Drelinkiewicz, A.; Socha, R.P.; Zimowska, M.; Lityńska-Dobrzyńska, L.; Bukowska, A. Solvent and substituent effects in hydrogenation of aromatic ketones over Ru/polymer catalyst under very mild conditions. *Molec. Catal.* **2019**, *470*, 145–151. [CrossRef]
58. Prymon, S.; Bukowska, A.; Bukowski, W.; Bester, K.; Hus, K.; Dychton, K.; Opiekun, Z. Effect of Fe₃O₄ particles on multi-hollow morphology of poly(HEMA-divinylbenzene-styrene) microspheres prepared by Pickering suspension polymerization. *Express Polym. Lett.* **2018**, *12*, 1026–1038. [CrossRef]
59. Sherrington, D.C. Preparation, structure and morphology of polymer supports. *Chem. Commun.* **1998**, *21*, 2275–2286. [CrossRef]
60. Zanini, M.; Marschelke, C.; Anachkov, S.E.; Marini, E.; Synytska, A.; Isa, L. Universal emulsion stabilization from the arrested adsorption of rough particles at liquid-liquid interfaces. *Nat. Commun.* **2017**, *8*, 15701. [CrossRef]
61. Lan, Y.; Caciagli, A.; Guidetti, G.; Yu, Z.; Liu, J.; Johansen, V.E.; Kamp, M.; Abell, C.; Vignolini, S.; Scherman, O.A.; et al. Unexpected stability of aqueous dispersions of raspberry-like colloids. *Nat. Commun.* **2018**, *9*, 3614. [CrossRef]

62. Binks, B.P. Particles as surfactants—similarities and differences. *Curr. Opin. Colloid Interface Sci.* **2002**, *7*, 21–41. [[CrossRef](#)]
63. De Carvalho-Guimarães, F.B.; Correa, K.L.; de Souza, T.P.; Amado, J.R.R.; Ribeiro-Costa, R.M.; Silva-Júnior, J.O.C. A review of pickering emulsions: Perspectives and application. *Pharmaceutics* **2022**, *15*, 141. [[CrossRef](#)]
64. Pan, J.; Chen, J.; Wang, X.; Wang, Y.; Fan, J.-B. Pickering emulsion: From controllable fabrication to biomedical application. *Interdiscip. Med.* **2023**, *1*, e20230014. [[CrossRef](#)]
65. Ortiz, D.G.; Pochat-Bohatier, C.; Cambedouzou, J.; Bechelany, M.; Miele, P. Current trends in pickering emulsions: Particle morphology and applications. *Engineering* **2020**, *6*, 468–482. [[CrossRef](#)]
66. Bukowska, A.; Bukowski, W.; Bester, K.; Flaga, S. Linkage of the PAMAM type dendrimer with the gel type resin based on glycidyl methacrylate terpolymer as a method of preparation of the polymer support for the recyclable palladium catalyst for Suzuki–Miyaura cross-coupling reactions. *RSC Adv.* **2015**, *5*, 49036–49044. [[CrossRef](#)]
67. Pretsch, E.; Bühlmann, P.; Badertscher, M. *Structure Determination of Organic Compounds Tables of Spectral Data*; Springer: Berlin/Heidelberg, Germany, 2009.
68. Martin, R.; Buchwald, S.L. Palladium-catalyzed Suzuki–Miyaura cross-coupling reactions employing dialkylbiaryl phosphine ligands. *Acc. Chem. Res.* **2008**, *41*, 1461–1473. [[CrossRef](#)]
69. Torborga, C.; Beller, M. Recent applications of palladium-catalyzed coupling reactions in the pharmaceutical, agrochemical, and fine chemical industries. *Adv. Synth. Catal.* **2009**, *351*, 3027–3043. [[CrossRef](#)]
70. Cho, S.H.; Kim, J.Y.; Kwak, J.; Chang, S. Recent advances in the transition metal-catalyzed twofold oxidative C–H bond activation strategy for C–C and C–N bond formation. *Chem. Soc. Rev.* **2011**, *40*, 5068–5083. [[CrossRef](#)]
71. Emadi, R.; Nekoo, A.B.; Molaverdi, F.; Khorsandi, Z.; Sheibani, R.; Sadeghi-Aliabadi, H. Applications of palladium-catalyzed C–N crosscoupling reactions in pharmaceutical compounds. *RSC Adv.* **2023**, *13*, 18715–18733. [[CrossRef](#)] [[PubMed](#)]
72. Seechurn, C.C.C.J.; Kitching, M.O.; Colacot, T.J.; Snieckus, V. Palladium-catalyzed cross-coupling: A historical contextual perspective to the 2010 Nobel Prize. *Angew. Chem. Int. Ed.* **2012**, *51*, 5062–5085. [[CrossRef](#)] [[PubMed](#)]
73. Blaser, H.-U.; Indolese, A.; Naud, F.; Nettekoven, U.; Schnyder, A. Industrial R&D on catalytic C–C and C–N coupling reactions: A personal account on goals, approaches and results. *Adv. Synth. Catal.* **2004**, *346*, 1583–1598.
74. Polshettiwar, V.; Len, C.; Fihri, A. Sustainable catalysts for cross-coupling reactions. *Coord. Chem. Rev.* **2009**, *253*, 2599–2626.
75. Mora, M.; Jiménez-Sanchidrián, C.; Ruiz, J.R. Recent advances in the heterogeneous palladium-catalysed Suzuki cross-coupling reaction. *Curr. Org. Chem.* **2012**, *16*, 1128–1150. [[CrossRef](#)]
76. Hussain, I.; Capricho, J.; Yawer, M.A. Synthesis of biaryls via ligand-free Suzuki–Miyaura cross-coupling reactions: A review of homogeneous and heterogeneous catalytic developments. *Adv. Synth. Catal.* **2016**, *358*, 3320–3349. [[CrossRef](#)]
77. Lawrence, A.S.; Martin, N.; Sivakumar, B.; Cirujano, F.G.; Dhakshinamoorthy, A. Palladium-based metal organic frameworks as heterogeneous catalysts for C–C couplings. *ChemCatChem* **2022**, *14*, e202200403. [[CrossRef](#)]
78. Martín, C.d.M.G.; García, J.I.H.; Bonardd, S.; Díaz, D.D. Lignin-based catalysts for C–C bond-forming reactions. *Molecules* **2023**, *28*, 3513. [[CrossRef](#)]
79. Sheikh, S.; Nasseri, M.A.; Chahkandi, M.; Reiser, O.; Allahresani, A. Dendritic structured palladium complexes: Magnetically retrievable, highly efficient heterogeneous nanocatalyst for Suzuki and Heck cross-coupling reactions. *RSC Adv.* **2022**, *12*, 8833–8840. [[CrossRef](#)]
80. Bester, K.; Bukowska, A.; Bukowski, W. Synthesis of gel-type imino-amino functionalized methacrylate-styrene terpolymers as supports for palladium catalysts for the Suzuki–Miyaura reaction. *Appl. Catal. A General* **2012**, *443*, 181–190. [[CrossRef](#)]

Disclaimer/Publisher’s Note: The statements, opinions and data contained in all publications are solely those of the individual author(s) and contributor(s) and not of MDPI and/or the editor(s). MDPI and/or the editor(s) disclaim responsibility for any injury to people or property resulting from any ideas, methods, instructions or products referred to in the content.